p15^{PAF} Is an Intrinsically Disordered Protein with Nonrandom Structural Preferences at Sites of Interaction with Other Proteins

Alfredo De Biasio,[†] Alain Ibáñez de Opakua,[†] Tiago N. Cordeiro,[‡] Maider Villate,[†] Nekane Merino,[†] Nathalie Sibille,[‡] Moreno Lelli,[§] Tammo Diercks,[†] Pau Bernadó,[‡] and Francisco J. Blanco[†¶]*

[†]Structural Biology Unit, Center for Cooperative Research in Biosciences (CIC bioGUNE), Derio, Spain; [‡]Centre de Biochimie Structurale, Institut National de la Santé et de la Recherche Médicale (INSERM) U1054, Centre National de la Recherche Scientifique (CNRS) UMR 5048, Université Montpellier 1 and 2, Montpellier, France; [§]Centre de Résonance Magnétique Nucléaire à Très Hauts Champs, Institut de Sciences Analytiques (CNRS/Ecole Normale Supérieure de Lyon/Université Claude Bernard Lyon 1), Villeurbanne, France; and [¶]IKERBASQUE, Basque Foundation for Science, Bilbao, Spain

ABSTRACT   We present to our knowledge the first structural characterization of the proliferating-cell-nuclear-antigen-associated factor p15^{PAF}, showing that it is monomeric and intrinsically disordered in solution but has nonrandom conformational preferences at sites of protein-protein interactions. p15^{PAF} is a 12 kDa nuclear protein that acts as a regulator of DNA repair during DNA replication. The p15^{PAF} gene is overexpressed in several types of human cancer. The nearly complete NMR backbone assignment of p15^{PAF} allowed us to measure 86 N-H^N residual dipolar couplings. Our residual dipolar coupling analysis reveals nonrandom conformational preferences in distinct regions, including the proliferating-cell-nuclear-antigen-interacting protein motif (PIP-box) and the KEN-box (recognized by the ubiquitin ligase that targets p15^{PAF} for degradation). In accordance with these findings, analysis of the ^{15}N R$_2$ relaxation rates shows a relatively reduced mobility for the residues in these regions. The agreement between the experimental small angle x-ray scattering curve of p15^{PAF} and that computed from a statistical coil ensemble corrected for the presence of local secondary structural elements further validates our structural model for p15^{PAF}. The coincidence of these transiently structured regions with protein-protein interaction and posttranslational modification sites suggests a possible role for these structures as molecular recognition elements for p15^{PAF}.

INTRODUCTION

p15^{PAF} is a 111-residue-long nuclear protein initially identified as a proliferating-cell-nuclear-antigen (PCNA)-binding protein in a yeast-two-hybrid screen (1). It binds to PCNA through its conserved PCNA-interacting protein motif (PIP-box). p15^{PAF} is a direct transcriptional target of the activating transcription factor 3, as well as the retinoblastoma/E2F pathway (2,3). It is targeted for degradation by the ubiquitin ligase anaphase-promoting complex/cyclosome (APC/C) and its coactivator Cdh1 through the conserved KEN-box motif at residues 78–80 (4). Independent of its APC destruction box, regulatory monoubiquitylation at residues K15 and K24 selectively occurs on PCNA-bound p15^{PAF} during the S phase (5). After ultraviolet (UV) stress, the interaction of monoubiquitylated p15^{PAF} with PCNA is disrupted, inducing recruitment of the translesion synthesis (TLS) polymerase η to PCNA at stalled replisomes and thus facilitating the bypass of replication-fork blocking lesions (5). Immunoprecipitation analysis and a mammalian two-hybrid assay indicate that p15^{PAF} binds the transactivation region of p53 and strongly inhibits its transcriptional activity (6). p15^{PAF} is overexpressed in multiple types of human cancer and is associated with poor prognosis (6–8). The structure of p15^{PAF} is un-

known, but the amino acid sequence suggests that it is intrinsically disordered.

Many proteins lack secondary and/or tertiary structure under physiological conditions, and these are referred to as intrinsically disordered proteins (IDPs) (9,10). It is now widely recognized that IDPs play diverse biological roles in all kingdoms of life (11). The majority of transcription factors (12) and proteins involved in signal transduction (13) in eukaryotes are predicted to be disordered or to contain long disordered segments. In addition, 79% of human-cancer-associated proteins have been classified as IDPs, compared to 47% of all eukaryotic proteins in the SWISS-PROT database (13). This observation underlines the importance of intrinsic disorder in the function of proteins that regulate processes often altered in cancer, such as cell proliferation, DNA repair, and apoptosis.

Structural analysis of IDPs is challenging, because their polypeptide backbone exhibits a high degree of flexibility due to rapid interconversion among multiple conformers. Because of this flexibility, NMR is the main method of choice for structural and functional studies of unfolded or partially folded proteins (14). Several NMR observables have been used to characterize IDPs (15). In particular, residual dipolar couplings (RDCs) measured in partially aligned media have been shown to be a sensitive tool for describing the conformational plasticity observed in IDPs. RDCs report on the specific dihedral angle space sampled at the residue level (16), and can be used to quantitatively estimate the population of secondary-structure elements or

Editor: David Eliezer.

long-range order (17). Conversely, small-angle x-ray scattering (SAXS) has the capacity to report on the three-dimensional space sampled by disordered states and therefore complements the local information provided by NMR (18,19). Integration of these experimental data into computational tools helps to elucidate the structure-function relationships for this important yet elusive class of proteins (20).

Here, we present to our knowledge the first structural characterization of human p15[PAF]. Although circular dichroism (CD) data and NMR chemical shifts are consistent with a largely disordered protein, backbone ^{15}N NMR relaxation and RDC measurements reveal the presence of transient nonrandom structural elements. Based on RDC data, sparsely populated helical structures localize in a central region of p15[PAF] that encompasses the PIP-box, whereas extended structures are present in regions at the C- and N-termini. The latter region includes residues K15 and K24, the sites for ubiquitylation that triggers the proteasome-dependent removal of p15[PAF] from the PCNA upon DNA-replication blockage. Our work identifies partially structured regions as potential molecular recognition elements for p15[PAF] and paves the way for further structural studies on the functional interactions of p15[PAF] with other proteins.

MATERIALS AND METHODS

Protein expression and purification

The DNA encoding human p15[PAF] with codon usage optimized for bacterial expression cloned into a pET11d vector was purchased from Entelechon. One liter of Luria broth or M9 minimal medium with the appropriate isotopic enrichment (1 g/L 99% [15]NH$_4$Cl or 2 g/L 97% [2]H$_7$, 99% [13]C$_6$-glucose or 2 g/L [1]H$_7$, or 99% [13]C$_6$-glucose or 2 g/L natural-abundance glucose, in 99.9% D$_2$O or in H$_2$O) containing 100 μg/mL ampicillin was inoculated with a clone of *Escherichia coli* BL21(DE3) cells transformed with the p15[PAF]-pET11d construct. Cells were grown at 37°C to an OD$_{600}$ of 0.6, and protein expression was induced with 1 mM isopropyl β-D-1-thiogalactopyranoside for 3 h at 37°C. Cells were harvested and resuspended in lysis buffer (20 mM Tris, pH 8.0, 1 mM dithiothreitol (DTT), and 1 mM EDTA plus one tablet of the protease inhibitor cocktail cOmplete (Roche, Basel, Switzerland) and sonicated on ice. Cells were pelleted by centrifugation at 25,000 rpm for 1 h at 4°C, and the supernatant was loaded on a Hiload 26/10 Q Sepharose column (GE Healthcare, Wauwatosa, WI) with a column volume (CV) of 53 mL. The column was washed with 20 mM Tris, pH 8.0, 1 mM DTT, and 1 mM EDTA (buffer A), and the protein was eluted with a two-step gradient using buffer A supplemented with NaCl up to 2 M total concentration (from 0% to 20% in 0.3 CV and from 20% to100% in 1 CV). Fractions containing the protein (as seen in SDS-PAGE) were pooled and prepared for reverse-phase chromatography by adding acetonitrile and trifluoroacetic acid (TFA) to final concentrations of 10% and 0.1%, respectively. Precipitated material was removed using a 0.22 μm filter and the clarified solution was then loaded on a Phenomenex Jupiter C$_{18}$ 250 × 10 mm column with 10 μm particles and a 300 Å pore diameter previously equilibrated with 10% aqueous acetonitrile and 0.1% TFA. The protein was eluted with a 10–40% gradient of elution buffer (90% aqueous acetonitrile and 0.1% TFA) in 5 CVs and freeze-dried. SDS-PAGE analysis showed that the protein coeluted with a p15[PAF] fragment that lacked the first 18 N-terminal residues, as identified by mass spectrometry. To remove this contaminant, a further step using a high-resolution Mono S HR 5/5 column (1 mL

CV, GE Healthcare) was applied. After solubilizing the freeze-dried material in water and adding the necessary reagents to match the composition of buffer A, p15[PAF] was injected into the column and eluted with a 0–30% NaCl gradient in 50 CVs using the same buffer plus 2 M NaCl. Mass spectrometry measurements indicated that the initial methionine was processed by bacterial enzymes. Protein concentration was determined by UV absorbance at 280 nm using the extinction coefficient calculated from the amino acid composition (8605 M^{-1}·cm^{-1}). The yield of pure protein was around 4 mg/L of Luria broth medium. The yields from cultures in minimal media were very variable, with a maximum of 2.5 mg/L. Protein samples were exchanged into different buffers using PD-10 desalting columns (GE Healthcare) and concentrated by ultrafiltration using Amicon devices with a 3 kDa cutoff.

SEC-MALLS

Size-exclusion chromatography-multiangle laser-light scattering (SEC-MALLS) experiments were performed at room temperature using a Superdex 200 10/300 GL column (GE HealthCare) connected to a DAWN-HELEOS light scattering detector and an Optilab rEX differential refractive index detector (Wyatt Technology, Santa Barbara, CA). The column was equilibrated with running buffer (phosphate-buffered saline (PBS), pH 7.0, 0.03% NaN$_3$, 0.1 μm filtered) and the SEC-MALLS system was calibrated with a sample of bovine serum albumin (BSA) at 1 g/L in the same buffer. A sample of 100 μL of p15[PAF] protein at 1 g/L was injected at 0.5 mL/min. Data acquisition and analysis employed ASTRA software (Wyatt). Based on numerous measurements on BSA samples at 1 g/L under the same or similar conditions, we estimate that the experimental error in molar mass is ~5%.

CD spectroscopy

The spectrum of a 50 μM sample of p15[PAF] in PBS (10 mM phosphate, 140 mM chloride, 153 mM sodium, and 4.5 mM potassium), pH 7.0, and 0.1 mM DTT was recorded on a Jasco-815 spectropolarimeter using a quartz cuvette (path length, 0.1 mm). Thermal denaturation was induced by heating (at a rate of 1°C/min) a sample of 7.0 μM p15[PAF] in the same buffer in a stoppered cuvette with 2 mm pathlength.

NMR spectroscopy

Unless otherwise indicated, NMR experiments were recorded at 25°C on a Bruker (Karlsruhe, Germany) Avance III spectrometer operating at 18.8 T (800 MHz of [1]H Larmor frequency) equipped with a TCI cryoprobe and *z* gradients. Spectra were processed with TopSpin NMR (Bruker) and analyzed using Sparky (21). [1]H chemical shifts were referenced directly, and ^{13}C and ^{15}N chemical shifts indirectly (22), to added 2,2-dimethyl-2-silapentane-5-sulfonate (DSS, methyl ^{1}H signal at 0.00 ppm). The experiments for spectral assignment were obtained using a 0.9 mM U-[^{13}C, ^{15}N] p15[PAF] sample in water with 5% (v/v) [2]H$_2$O and 2 mM DTT, pH 6.3 adjusted with concentrated HCl and NaOH. [1]H^N, ^{15}N, [13]C′, [13]C$^\alpha$, [13]C$^\beta$ and [1]H$^\alpha$ assignments were obtained from the analysis of two-dimensional [1]H-^{15}N heteronuclear single quantum coherence (HSQC) and ^{1}H-^{13}C HSQC, and three-dimensional HNCO, HN(CA)CO, HNCACB, HN(CO) CACB, HNCA, HN(CO)CA, HN(CA)HA, HN(COCA)HA, and (H) C(CCO)NH experiments. A partial automatic assignment of the backbone and [13]C$^\beta$ resonances was obtained with the program MARS (23) and was manually completed. Side-chain amide groups were assigned using the HNCO, HN(CO)CACB, and HN(CO)CA spectra. Several H$^\alpha$ assignments were obtained or confirmed in the ^{1}H-^{13}C HSQC spectrum. The assignment has been deposited in the BioMagResBank (BMRB ID 19332).

[1]H-^{15}N RDCs were measured on a 100 μM U-[^{2}H, ^{13}C,^{15}N]-labeled p15[PAF] sample in 200 mM sodium 2-(N-morpholino)ethanesulfonate

(MES), pH 6.0, and 1 mM DTT at 25°C aligned partially in a stretched poly-acrylamide gel yielding 3.2 Hz splitting of the ^{2}H$_2$O signal. The gel was prepared with 6% w/v acrylamide and a molar acrylamide/N,N'-methylene-bisacrylamide ratio of 83:1. A commercial apparatus (Cortecnet, Paris, France) was used for stretching the gel and inserting it into an open-ended 5 mm NMR tube (24). To overcome the typical overlap problems in the two-dimensional ^{1}H-^{15}N HSQC of this IDP, we employed a modified three-dimensional HNCO transverse relaxation-optimized spectroscopy (TROSY) experiment to resolve and measure a maximal number of ^{1}H-^{15}N RDCs. In this experiment, TROSY and semi-TROSY (in H^N) sub-spectra were recorded in an interleaved manner and with high resolution (2.5 Hz, interpolated to 0.4 Hz in processing) in the direct ^{1}H dimension; ^{1}H-^{15}N RDCs were then derived from the separation between correspond-ing spin-state-selective HN$^\alpha$ and HN$^\beta$ signals.

The secondary chemical shift values were calculated taking the difference between experimentally measured ^{1}H$^\alpha$, ^{13}C', ^{13}C$^\alpha$, ^{13}C$^\beta$ chemical shifts and their amino-acid-specific random-coil values. Nearest-neighbor amino acid sequence corrections were introduced in the calculations of the p15^{PAF} chemical shift deviations from the reference values as described in the original reports.

Backbone amide ^{15}N transverse (T$_2$) relaxation measurements were acquired at 25°C on a Bruker Avance III spectrometer operating at 23.4 T (1.0 GHz and 101.4 MHz of ^{1}H and ^{15}N Larmor frequencies, respectively) equipped with a TCI cryoprobe and z-gradients. A sample of 180 μM [U-^{15}N]-p15^{PAF} in 200 mM MES, pH 6.8, 0.5 mM DTT, and 5% ^{2}H$_2$O with added protease inhibitors (Roche) was used. The pulse sequence for ^{1}H-de-tected ^{15}N T$_2$ relaxation measurement (25) recorded a series of two-dimen-sional ^{1}H-^{15}N correlation maps modulated by different ^{15}N T$_2$ relaxation delays in a fully interleaved mode. This reduces sources of error from envi-ronmental fluctuations during acquisition. The ^{15}N T$_2$ relaxation delays were 16.96, 33.92, 50.88, 84.80, 118.72, 169.60, 220.48, and 254.40 ms. Each ^{1}H-^{15}N correlation map was acquired with 48 scans and 2.5 s of recycle delay, 2048 direct complex points, and 64 indirect complex points with an echo/antiecho acquisition scheme. The acquisition times were $t_{1max} = 33.6$ ms and $t_2 = 78.6$ ms for the indirect and direct dimensions, respectively.

RDC analysis

Ensembles of explicit models were generated for p15^{PAF} using Flexible-Meccano, an algorithm that sequentially builds chains of peptide planes based on amino-acid-specific conformational propensity and volume exclu-sion (17). This algorithm has been shown to adequately sample the confor-mational space for unfolded proteins using randomly selected pairs of dihedral φ,ψ angles derived from coil regions in high-resolution structures. To account for deviations from the random-coil description of p15^{PAF} conformational sampling, different structure ensembles were computed including user-defined local conformational propensities in continuous regions of the protein. Canonical secondary-structure backbone dihedral an-gles were used except in the KEN-box, where the φ,ψ angles were taken from the corresponding region in the crystal structure of the protein Mad3 in the crystal structure of the mitotic checkpoint complex (PDB entry 4AEZ). All ensembles comprised 100,000 conformers. For each conformer in a particular ensemble, the ^{1}H-^{15}N RDCs were predicted by PALES (26), and the per-residue averages over all conformers were computed and defined as the simulated RDC values. The quality of each ensemble was assessed by comparing the simulated and experimental values through a figure of merit:

$$\chi^2 = \frac{1}{N} \sum \left(RDC_{exp} - \kappa RDC_{sim} \right)^2,$$

where RDC$_{exp}$ and RDC$_{sim}$ are the experimentally measured and simulated RDC values, respectively, and N is the number of analyzed RDCs. All back-calculated RDC$_{sim}$ values were scaled uniformly by a factor κ to account for the uncertainty in the degree of sample alignment.

Small-angle x-ray scattering

These measurements were carried out at the European Molecular Biology Laboratory BioSAXS beamline X33 at the DORIS Storage Ring, DESY (Hamburg, Germany), using an x-ray wavelength of 1.54 Å and a sam-ple-to-detector distance of 2.7 m (27). p15^{PAF} samples were measured at 25°C at concentrations of 4.9, 2.9, 2.0, and 1.0 g/L in PBS, pH 7.0, and 1 mM DTT. The scattering patterns of the buffer solutions were recorded before and after the measurements of each protein sample. The scattering profiles measured covered a momentum transfer range of $0.0087 < s < 0.60$ Å^{-1}. Inspection of the consecutive 30 s x-ray exposures confirmed that no radiation damage was present. Final curves at each concentration were derived after the averaged buffer patterns were subtracted from the protein sample patterns using standard protocols with PRIMUS (28). No sign of aggregation was observed in any of the curves. In addition, no concentration effects were observed in the data sets, indicating the absence of oligomerization equilibria. Consequently, the curve at the highest concentration, 4.9 g/L, was used for further analysis. The forward scattering intensity, $I(0)$, and the radius of gyration, R_g, were evaluated using Guinier's approximation (29), assuming that at very small angles ($s < 1.3/R_g$), the intensity can be well represented as $I(s) = I(0) \exp(-(sR_g)^2/3)$. Molecular weight estimation for p15^{PAF} was performed using a BSA sample at 3.71 g/L as a reference. The pairwise distance distribution function, $p(r)$, and the maximum particle dimension, D_{max}, were computed with the program GNOM (30), using a momentum transfer range of $0.015 < s < 0.40$ Å^{-1}.

For the simulation of the SAXS curves from RDC-derived ensemble models, side chains were added to each of the conformers using SCCOMP (31) and the scattering intensity of each conformer was calculated using CRYSOL (32). Then, the individual SAXS curves were averaged to yield the ensemble scattering curve. Both curves were directly compared by scaling the theoretical curve using a momentum transfer range of $0.015 < s < 0.50$ Å^{-1}. Constant subtraction was used. A total of 4000 struc-tures were used to calculate the average curve, which was sufficient to attain convergence. The coordinates of this ensemble have been deposited in the Protein Ensemble Database (pE-DB) (33) with accession code 6AAA.

RESULTS

Sequence analysis and disorder prediction

The amino acid composition of p15^{PAF} shows a low content of structure-promoting residues (5.4% aromatic and 12.6% aliphatic amino acids) and a high content of disorder-promoting ones (30.6% charged amino acids), a feature typical for IDPs (34). The disorder prediction for p15^{PAF} was made using the metaPrDOS web server, which inte-grates the results of eight different methods (35). The two-state prediction output (unfolded versus folded) is consistent with p15^{PAF} being largely unstructured, with the exception of residues 51–70, which encompass the PIP-box motif at residues 62–69 (Fig. 1). The pattern of the PIP-box sequence is *QXXhXXaa*, where *h* is an aliphatic hydrophobic residue (most frequently I, L, or M), *a* is an aromatic hydrophobic residue (F, W, or Y), and *X* is any of the 20 proteinogenic amino acids, and is strictly conserved in p15^{PAF}. An N-ter-minal region centered at V17 and A18 is predicted to have reduced disorder tendency, suggesting that it may have some propensity to form transient nonrandom structures. This region includes monoubiquitylation sites at residues K15 and K24. The sequence of p15^{PAF} protein contains
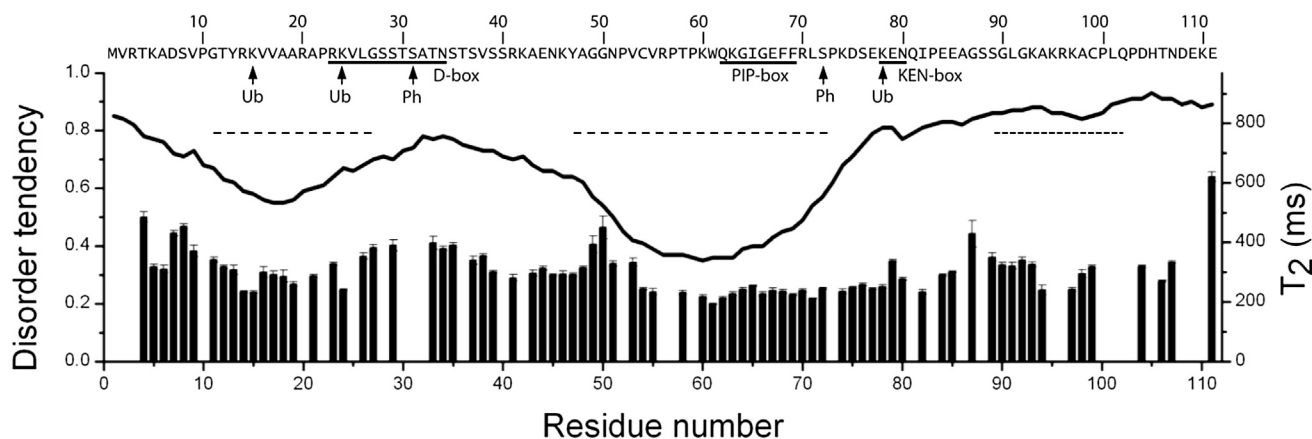
FIGURE 1   Amino acid sequence features and backbone dynamics of p15[PAF]. Sites of ubiquitylation (*Ub*) or phosphorylation (*Ph*) are indicated by arrows. Residues encompassing the conserved D-box, PIP-box, and KEN-box motifs are underlined. The solid line shows the disorder prediction by the metaPrDOS server (*left axis*) and dotted lines indicate the protein interaction regions predicted by ANCHOR (using a threshold of 0.5). Bars indicate the backbone amide ^{15}N T_2 relaxation times at 25°C and 23.4 T (*right axis*).

a cyclin-dependent kinase phosphorylation consensus sequence (residues 72 and 73) and two targeting signals for the ubiquitin ligase Cdh1-APC complex: a destruction box (D-box, with the *RXXLXXXXN* consensus sequence) at residues 23–34 (36), and a KEN-box at residues 78–80 (37). Interestingly, prediction of protein binding regions using the web server ANCHOR (38) identifies three sequence segments (11–27, 47–73, and 89–102), two of which correspond to regions with reduced disorder tendencies.

Cloning, expression, and purification

The polypeptide studied here corresponds to p15[PAF] isoform 1, the canonical sequence comprising the full-length protein (Uniprot Q15004) coded by the human KIAA0101 gene. No additional residues that could perturb the native structural features of this putative IDP were introduced. Since no affinity tag was used, high expression levels of the recombinant gene were necessary for efficient protein purification. Considering that the human cDNA sequence coded seven of the eight arginine residues with codons that are at low abundance in *E. coli*, a synthetic gene with codons optimized for bacterial expression was used. Protein p15[PAF] was then purified by three sequential chromatographic separations. As frequently occurs with recombinant gene expression in bacteria, the initial methionine was processed and the purified protein consists predominantly of residues 2–111 of p15[PAF], with a small amount (~10%) of the intact chain.

Structural analysis by SEC-MALLS and CD

The protein eluted from the SEC column at a volume that, according to the calibration with molecular weight standards, corresponds to an apparent molar mass of 25 kDa. However, the mass derived from the MALLS data is 11.5 kDa (Fig. 2 *A*), demonstrating that p15[PAF] is monomeric. These inconsistent results suggest that p15[PAF] is either folded with an elongated shape or is flexible and disordered (39). In both instances, it would elute at a smaller volume than a globular protein of the same mass.

The far-UV CD spectrum of p15[PAF] shows a minimum at 198 nm and a shoulder at 222 nm, consistent with a predominantly random-coil protein with little secondary structure (Fig. 2 *B*). The thermal denaturation curve of p15[PAF] followed by the changes in the CD signal at 222 nm (see Fig. 2 *B*, *inset*) does not show any cooperative folding-unfolding transition, indicating that p15[PAF] lacks a defined tertiary structure.

NMR assignment and analysis

The resonances of the p15[PAF] backbone nuclei and the aliphatic side-chain carbon resonances were assigned using conventional triple resonance spectra with amide proton signal detection. For the two initial N-terminal residues (V2 and R3), no crosspeaks were observed in the ^{1}H–^{15}N HSQC spectrum. For the 99 remaining nonproline residues, all the ^{1}H-^{15}N correlation signals could be unambiguously assigned (Fig. 3). The p15[PAF] protein contains nine proline residues whose preceding peptide bond is in the *trans* configuration, as inferred by the differences in the proline C^{β} and C^{γ} chemical shifts (40). A few signals with ~5% the intensity of the major ones are observed in the ^{1}H-^{15}N HSQC spectrum (data not shown). At least four of these signals correspond to residues preceded by a proline with $^{13}C^{\beta}$ and $^{13}C^{\gamma}$ chemical shifts typical for the *cis* configuration. Therefore, we interpret them as arising from small populations of p15[PAF] molecules with *cis* isomers at some of the peptidyl-prolyl peptide bonds.

The lack of dispersion in the backbone amide ^{1}H chemical shifts as seen in the ^{1}H-^{15}N HSQC spectrum gives
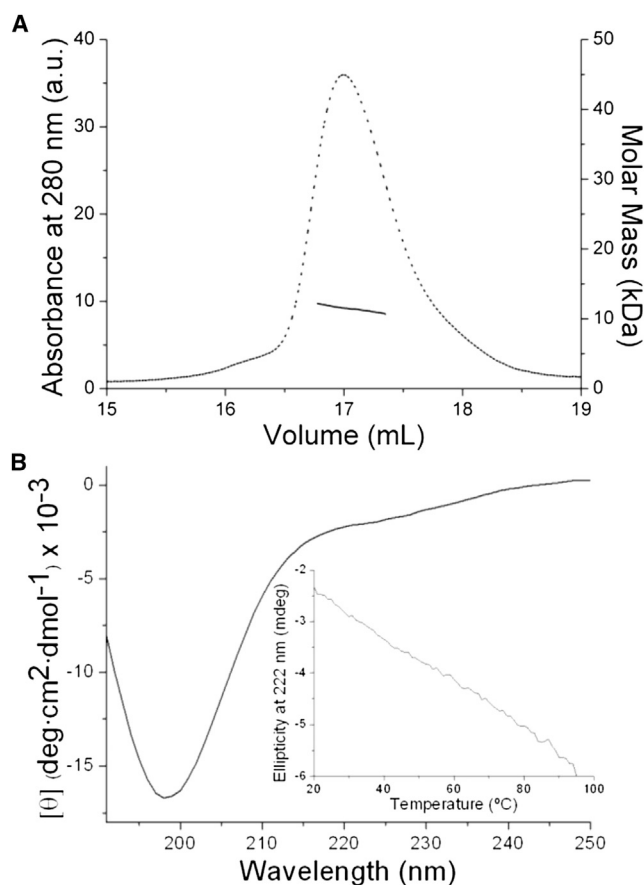
FIGURE 2 p15^{PAF} is monomeric and has little structure in solution. (*A*) Size-exclusion chromatogram of p15^{PAF} in PBS, pH 7.0, at room temperature (*dotted line* and *left axis*), and molar mass derived from MALLS (*solid line* and *right axis*). (*B*) CD spectrum of p15^{PAF} in PBS, pH 7.0, at 25°C. (*Inset*) Thermal denaturation as measured by changes in the signal at 222 nm.

evidence of the largely disordered and flexible nature of p15^{PAF} under native conditions. The average ^{15}N transverse relaxation time (T$_2$) measured at 25°C and 23.4 T is ~300 ms, similar to the reported values for a disordered protein from measles virus at the same temperature and magnetic field strength (41). However, several regions of p15^{PAF} show relatively short T$_2$ values (Fig. 1), and two of them correspond to sequences with reduced predicted disorder tendency. A shorter-than-average T$_2$ might indicate restricted local flexibility on a fast timescale (nanoseconds to picoseconds) or conformational motions on a slow timescale (microseconds to milliseconds) that typically engulf several contiguous residues. However, either interpretation points to the same result: the rather unrestricted and disconnected flexibility characteristic of IDPs is somewhat altered toward more restricted and connected mobility. There is a certain correlation between local residue bulkiness and transverse relaxation rates R$_2$ (the inverse of T$_2$; see Fig. S1 in the Supporting Material), suggesting that local restrictions in polypeptide chain dynamics can be explained in part by steric interactions between side chains and the backbone, as found for other IDPs (42).

Chemical shift deviations from random-coil values were computed using four different sets of reference values. Three sets were experimentally obtained from small disordered peptides (43–45). The fourth is a set of values derived from the NMR assignments of 14 IDPs under native conditions (46). At the level of sensitivity of chemical shifts, this analysis did not provide consistent evidence of preferred conformations in p15^{PAF}, suggesting that its behavior is close to that of a random coil. The deviations calculated for the H$^\alpha$, C′, C$^\alpha$, and C$^\beta$ nuclei using one of the peptide-derived data sets and the IDP-derived data set are shown in Fig. S2.

^{1}H-^{15}N RDCs of p15^{PAF} measured in a stretched poly-acrylamide gel aligning medium are mainly negative (Fig. 4, *black circles*), as observed in disordered proteins (16,47). As RDC variations in unfolded proteins are mainly dictated by the steric hindrance between neighboring residues, the RDC profile is also sequence-specific, with larger RDCs observed where bulky amino acids are present (42). To assess whether any nonrandom structure is present in p15^{PAF}, we looked for deviations in the RDC experimental profile from the behavior expected for a random coil with the p15^{PAF} sequence. For that purpose, we applied the Flexible Meccano approach (48) to build ensembles of p15^{PAF} models with randomly selected torsion angle pairs drawn from a database of amino-acid-specific conformations present in loop regions of high-resolution x-ray structures (17). The alignment tensor was predicted for each conformer using PALES (26), and the associated RDCs were calculated for each ^{1}H-^{15}N vector with respect to this tensor. RDCs from each site were then averaged over 100,000 conformers to ensure convergence. The values calculated from this statistical coil ensemble (Fig. 4, *blue line*) were then compared to the experimental RDCs. Three regions are identified in the p15^{PAF} sequence for which there is a disagreement between the experimental and calculated RDCs: a central region (residues 54–69), an N-terminal region (residues 15–24), and a C-terminal region (residues 94–104). Since the random-coil model did not fully reproduce the measured RDCs, different structurally biased ensembles of 100,000 conformers were computed by systematically forcing distinct secondary-structure populations within the p15^{PAF} sequence. These ensembles were quantitatively evaluated by comparison of the predicted RDCs with the experimental ones. The best agreement was found by imposing 15% α-helix and 3$_{10}$ helix in residues 54–60 and 67–69, respectively, and 8% β-strand in residues 15–24 and 94–104 (Fig. 4, *red line*). The correlation between calculated and measured RDCs was further improved by introducing 15% of torsion angles for canonical inverse γ-turn structure in W61, and 5% of KEN-box torsion angles in p15^{PAF} residues 76–80. These angles were taken from the KEN-box-containing segment
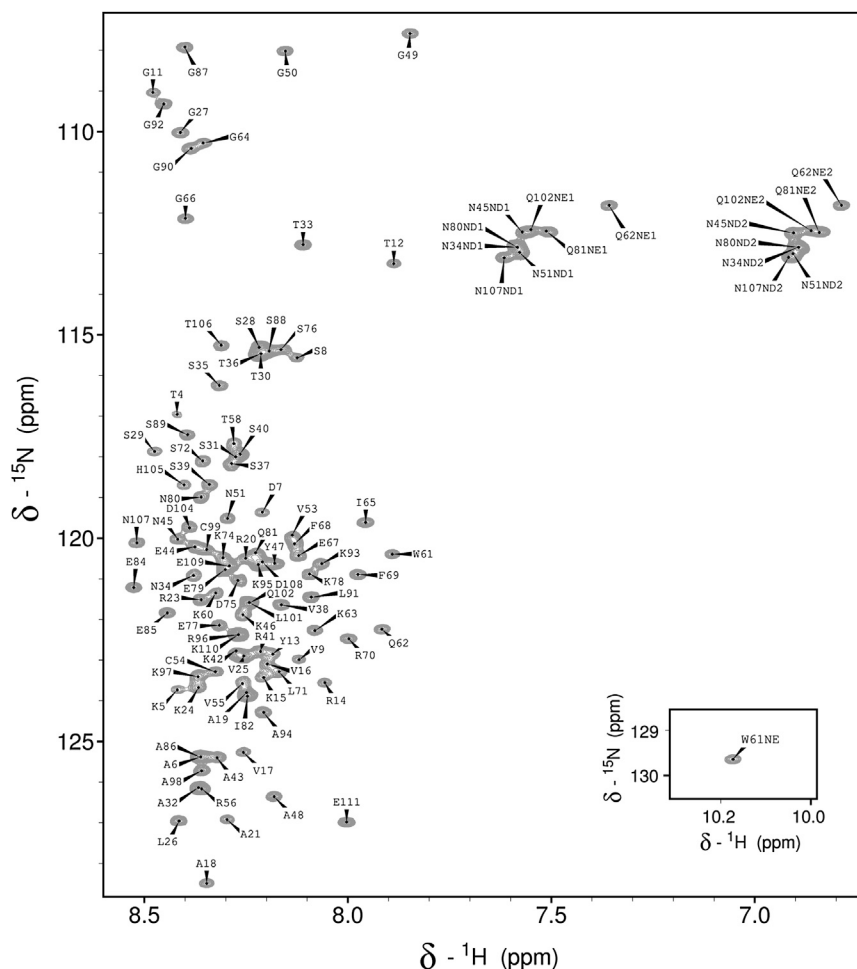
FIGURE 3 Residue-specific assignment of the ^1H-^{15}N HSQC NMR spectrum of p15^{PAF} at pH 6.3 and 25°C. The pairs of signals from the side-chain amides of asparagine and glutamine residues are arbitrarily labeled ND1/ND2 and NE1/NE2, respectively, without implying a stereospecific assignment. (*Inset*) Signal from the W61 indole group.

(residues 18–22) of the mitotic spindle assembly checkpoint protein Mad3 bound to the APC/C coactivator protein CdC20 (49). Introduction of these secondary-structure preferences in the indicated regions not only results in a notable agreement with the measured RDCs in those regions but also improves the correlation along the entire chain.

SAXS analysis

We used SAXS to characterize the conformational space sampled by p15^{PAF} in solution and to validate the structure ensemble derived from the RDC data. As shown in Fig. 5, the SAXS profile of p15^{PAF} and its Kratky representation are typical for a disordered protein. The SAXS curve shows no features (Fig. 5 *A*) and the Kratky plot does not show a maximum, with a monotonic increase at large momentum transfer values (Fig. 5 *B*). Analysis of the smallest angles by Guinier's approach using a momentum transfer range of $sR_g < 1.3$ (where s is the momentum transfer and R_g is the radius of gyration) indicates the presence of a particle with $R_g = 28.1 \pm 0.3$ Å and an estimated molecular mass of 12.6 kDa. The latter is in excellent agreement with the calculated molar mass of 11.9 kDa for the p15^{PAF} monomer.

The R_g of p15^{PAF} is slightly smaller than expected for a 110-residue-long random-coil polypeptide ($R_g^{RC} = 29.5$ Å), suggesting that p15^{PAF} could transiently adopt a less extended structure (50). The disordered nature of p15^{PAF} is substantiated by the large value of the maximum particle dimension ($D_{max} = 120 \pm 10$ Å). The average of the scattering curves and the Kratky plots calculated for the 4000 conformations that best explain the RDC measurements are represented by black lines in Fig. 5. The experimental SAXS data were accurately reproduced by those calculated for the ensemble of p15^{PAF} models, indicating that this ensemble is a good representation of the conformational distribution of p15^{PAF} in solution.

DISCUSSION

Our SEC-MALLS, CD, SAXS, and NMR measurements show that p15^{PAF} is monomeric in solution, with no tertiary structure and few conformational preferences. Its large conformational heterogeneity makes a detailed structural characterization of this IDP challenging, since experimental data are ensemble-averaged (51). Validating the combined local structural information from RDCs and
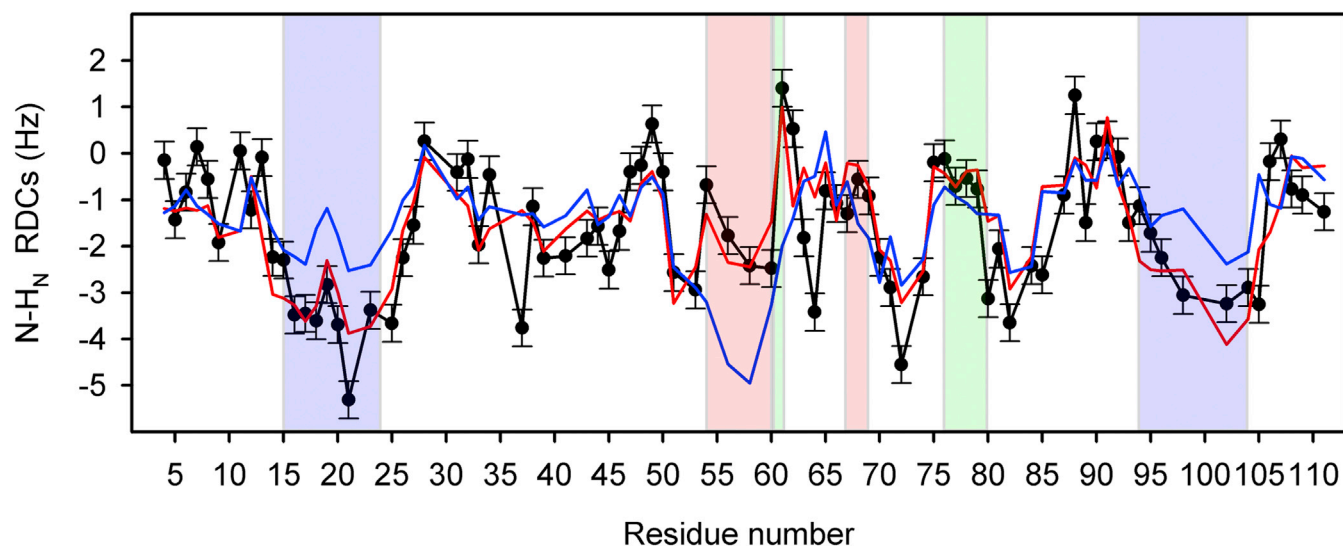
FIGURE 4 Local nonrandom structures in the conformational ensemble of p15^{PAF}. Comparison of the experimental RDCs (*black circles*) with those simulated using a random-coil ensemble without any structural bias (*blue line*) and those calculated including the conformational preferences described in the text (*red line*). The estimated error in the measured RDCs is ± 0.4 Hz (indicated by the error bars). Calculated RDCs are plotted only if the corresponding experimental value was available. Those regions where nonrandom structures were detected are shaded in blue (extended structure), red (helical structure), or green (inverse γ-turn and KEN-box structures). To see this figure in color, go online.

global shape information provided by SAXS against computer-generated conformational ensembles has been a powerful approach in performing this demanding task ([52]). Chemical-shift analysis alone did not consistently detect nonrandom regions, whereas analysis of the backbone amide RDCs precisely indicated specific regions in p15^{PAF} that significantly deviate from random-coil structure. We do not fully understand the origin of this apparent contradiction, but we think that it may be because 1), p15^{PAF} contains very little nonrandom structure; 2), the quality of the available random-coil chemical-shift reference data sets limits the detection of these low populations of nonrandom structures; 3), the reference RDC values calculated for a sufficiently large random-coil ensemble allow more sensitive detection of nonrandom structures. The latter two reasons may be especially relevant in the case of p15^{PAF} due to an unknown property feature of this protein.

As anticipated by disorder-tendency predictions, the central p15^{PAF} region encompassing residues 54–69 shows the major deviations from a random coil. Within this region, residues ^{67}EFF^{69} have detectable 3_{10} helical propensities. These three residues are C-terminal in the conserved PIP-box motif of p15^{PAF} that mediates its binding to PCNA. Our analysis also shows that the RDC deviations of the eight residues preceding the PIP-box (^{54}CVRPTPKW^{61}) can be explained by a larger-than-random propensity for α-helical dihedral angles in residues 54–60 and γ-turn angles in W61. The detection of helical structure in this region may be surprising at first, given the presence of two prolines. However, RDCs report on time- and ensemble-averaged conformations that do not necessarily imply a continuous

eight-residue-long helical structure as the major nonrandom conformation. Prolines generally destabilize α-helical (and β-strand) structures, but they can nevertheless be accommodated, and may even be preferred as N-capping residues in a helix ([53]). Further nonrandom local structure was detected in the N- and C-terminal regions of p15^{PAF}, and within the KEN-box motif (residues 78–80).

The functional advantage of IDPs presumably derives from their conformational versatility, allowing for interactions with different ligands, and for extensive regulation through posttranslational modifications at many accessible sites ([54]). Many IDPs fold upon binding to their partners ([55]). This may occur via 1), induced fit, in which the binding partner induces the disordered protein to adopt the bound-state conformation; 2), conformational selection, in which the binding partner selects a binding-efficient conformation from the ensemble sampled in the free state; or 3), a mixture of induced fit and conformational selection ([56,57]).

Several reports in the literature show that p15^{PAF} interacts with other proteins. Based on results of yeast two-hybrid and coimmunoprecipitation experiments using wild-type and mutant p15^{PAF} expressed in mammalian cells, Yu et al. ([1]) assert that p15^{PAF} interacts with PCNA through its PIP-box. Liu and colleagues ([6]) report, based on their coimmunoprecipitation and two-hybrid experiments, that p15^{PAF} interacts with p53, although the interaction sites are unknown. And based on the increased protein levels in null-Cdh1 cells, and using KEN-box mutants, Emanuele et al. ([4]) report that p15^{PAF} interacts with APC/C-Cdh1 through its KEN-box. However, none of these interactions has been validated by structural and/or quantitative experimental methods using pure proteins ([58]).
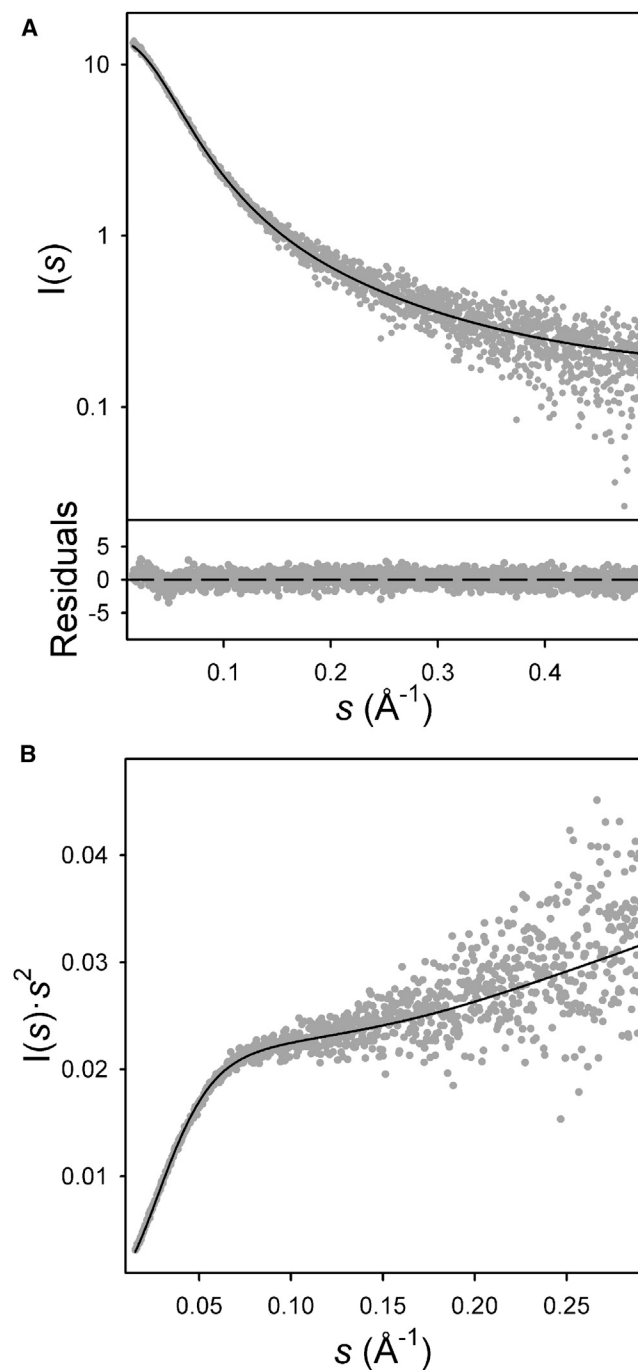
FIGURE 5 SAXS data and analysis of p15^{PAF} in PBS, pH 7.0, at 25°C. (*A*) Semilogarithmic representation of SAXS intensity versus momentum transfer (*gray circles*), and the back-calculated curve derived from the conformational ensemble that best explains the experimental RDCs (*solid black line*). The residuals of the fitting are shown below (*dashed line and gray circles*). (*B*) Kratky plot of the data shown in *A*.

In all of the crystal structures of PIP-box peptides or proteins bound to PCNAs reported in the literature, both conserved aromatic residues of the PIP-box bind to the same hydrophobic groove on the PCNA surface and are part of a 3$_{10}$ helical turn (59–64). If the PIP-box residues

of p15^{PAF} bind to PCNAs in the same conformation as seen in homologous structures, a conformational selection mechanism might contribute to the binding. However, to confirm and evaluate the extent of this possible contribution relative to an induced-fit mechanism, it would be necessary to determine the p15^{PAF}/PCNA complex structure and describe the different populations and kinetic rates for both mechanisms (65). The preference for helical structure in the eight residues preceding the PIP-box may represent their PCNA-bound conformation, providing further contacts beyond the strict PIP-box. These residues N-terminal to the PIP-box are not conserved in PCNA interacting proteins. In the crystal structures of peptides bound to PCNAs, only a few residues preceding the PIP-box sequence are seen, and these adopt an extended structure. However, in the structures of both the full-length human flap endonuclease 1 protein bound to PCNA (64) and the yeast replication factor C bound to yeast PCNA (59), some of the nonconserved residues N-terminal to the PIP-box fold into a helical structure (but there is no proline in either of these PCNA-bound sequences). In the KEN-box and the N-terminal region, there are three lysines (K15, K24, and K78) that are known targets of regulatory ubiquitylation. The observed preferred conformations in these regions may play a role in the recognition by the ubiquitylation complex. In this context, it is interesting to note that monoubiquitylation at K15 and K24 of chromatin-associated p15^{PAF} is templated through PCNA binding (5), and that ubiquitylation sites tend not to be located in disordered regions (66). It is tempting to speculate that binding to PCNAs may stabilize the observed local structure and/or induce additional structure around K15 and K24 that facilitates the recognition of p15^{PAF} as a target for ubiquitylation.

The cyclin-dependent kinase inhibitor p21^{CIP1} is another IDP that interacts with diverse ligands via distinct regions and competes with p15^{PAF} for PCNA binding through its PIP-box (1). However, a detailed conformational analysis of p21^{CIP1} has been hampered by the low solubility of this protein, and only small fragments have been studied (67). Our work on full-length p15^{PAF} paves the way for further structural studies on its interactions with physiological partners.

SUPPORTING MATERIAL

Two figures are available at http://www.biophysj.org/biophysj/supplemental/S0006-3495(14)00072-1.

REFERENCES

1. Yu, P., B. Huang, …, Y. Luo. 2001. p15(PAF), a novel PCNA associated factor with increased expression in tumor tissues. *Oncogene.* 20:484–489.

2. Turchi, L., M. Fareh, …, T. Virolle. 2009. ATF3 and p15PAF are novel gatekeepers of genomic integrity upon UV stress. *Cell Death Differ.* 16:728–737.

3. Chang, C. N., M. J. Feng, …, Y. M. Jeng. 2013. p15^{PAF} is an Rb/E2F-regulated S-phase protein essential for DNA synthesis and cell cycle progression. *PLoS ONE.* 8:e61196.

4. Emanuele, M. J., A. Ciccia, …, S. J. Elledge. 2011. Proliferating cell nuclear antigen (PCNA)-associated KIAA0101/PAF15 protein is a cell cycle-regulated anaphase-promoting complex/cyclosome substrate. *Proc. Natl. Acad. Sci. USA.* 108:9845–9850.

5. Povlsen, L. K., P. Beli, …, C. Choudhary. 2012. Systems-wide analysis of ubiquitylation dynamics reveals a key role for PAF15 ubiquitylation in DNA-damage bypass. *Nat. Cell Biol.* 14:1089–1098.

6. Liu, L., X. Chen, …, F. Zhu. 2012. Variant 1 of KIAA0101, overexpressed in hepatocellular carcinoma, prevents doxorubicin-induced apoptosis by inhibiting p53 activation. *Hepatology.* 56:1760–1769.

7. Hosokawa, M., A. Takehara, …, H. Nakagawa. 2007. Oncogenic role of KIAA0101 interacting with proliferating cell nuclear antigen in pancreatic cancer. *Cancer Res.* 67:2568–2576.

8. Kato, T., Y. Daigo, …, M. Kaji. 2012. Overexpression of KIAA0101 predicts poor prognosis in primary lung cancer patients. *Lung Cancer.* 75:110–118.

9. Dyson, H. J., and P. E. Wright. 2005. Intrinsically unstructured proteins and their functions. *Nat. Rev. Mol. Cell Biol.* 6:197–208.

10. Uversky, V. N. 2002. Natively unfolded proteins: a point where biology waits for physics. *Protein Sci.* 11:739–756.

11. Ward, J. J., J. S. Sodhi, …, D. T. Jones. 2004. Prediction and functional analysis of native disorder in proteins from the three kingdoms of life. *J. Mol. Biol.* 337:635–645.

12. Liu, J., N. B. Perumal, …, A. K. Dunker. 2006. Intrinsic disorder in transcription factors. *Biochemistry.* 45:6873–6888.

13. Iakoucheva, L. M., C. J. Brown, …, A. K. Dunker. 2002. Intrinsic disorder in cell-signaling and cancer-associated proteins. *J. Mol. Biol.* 323:573–584.

14. Dyson, H. J., and P. E. Wright. 2004. Unfolded proteins and protein folding studied by NMR. *Chem. Rev.* 104:3607–3622.

15. Marsh, J. A., and J. D. Forman-Kay. 2011. Ensemble modeling of protein disordered states: Experimental restraint contributions and validation. *Proteins.* 80:556–572.

16. Louhivuori, M., K. Pääkkönen, …, A. Annila. 2003. On the origin of residual dipolar couplings from denatured proteins. *J. Am. Chem. Soc.* 125:15647–15650.

17. Bernadó, P., L. Blanchard, …, M. Blackledge. 2005. A structural model for unfolded proteins from residual dipolar couplings and small-angle x-ray scattering. *Proc. Natl. Acad. Sci. USA.* 102:17002–17007.

18. Bernadó, P., E. Mylonas, …, D. I. Svergun. 2007. Structural characterization of flexible proteins using small-angle x-ray scattering. *J. Am. Chem. Soc.* 129:5656–5664.

19. Sibille, N., and P. Bernadó. 2012. Structural characterization of intrinsically disordered proteins by the combined use of NMR and SAXS. *Biochem. Soc. Trans.* 40:955–962.

20. Mittag, T., and J. D. Forman-Kay. 2007. Atomic-level characterization of disordered protein ensembles. *Curr. Opin. Struct. Biol.* 17:3–14.

21. Goddar, T. D., and D. G. Kneller. 2008. Sparky: NMR Assignment and Integration Software. http://www.cgl.ucsf.edu/home/sparky/.

22. Wishart, D. S., C. G. Bigam, …, B. D. Sykes. 1995. ^{1}H, ^{13}C and ^{15}N chemical shift referencing in biomolecular NMR. *J. Biomol. NMR.* 6:135–140.

23. Jung, Y. S., M. Sharma, and M. Zweckstetter. 2004. Simultaneous assignment and structure determination of protein backbones by using NMR dipolar couplings. *Angew. Chem. Int. Ed. Engl.* 43:3479–3481.

24. Chou, J. J., S. Gaemers, …, A. Bax. 2001. A simple apparatus for generating stretched polyacrylamide gels, yielding uniform alignment of proteins and detergent micelles. *J. Biomol. NMR.* 21:377–382.

25. Farrow, N. A., R. Muhandiram, …, L. E. Kay. 1994. Backbone dynamics of a free and phosphopeptide-complexed Src homology 2 domain studied by ^{15}N NMR relaxation. *Biochemistry.* 33:5984–6003.

26. Zweckstetter, M. 2008. NMR: prediction of molecular alignment from structure using the PALES software. *Nat. Protoc.* 3:679–690.

27. Round, A. R., D. Franke, …, M. Roessle. 2008. Automated sample-changing robot for solution scattering experiments at the EMBL Hamburg SAXS station X33. *J. Appl. Crystallogr.* 41:913–917.

28. Konarev, P. V., V. V. Volkov, …, D. I. Svergun. 2003. PRIMUS: a Windows PC-based system for small-angle scattering data analysis. *J. Appl. Crystallogr.* 36:1277–1282.

29. Guinier, A. 1939. X-ray diffraction at small angles. Application to the study of ultramicroscopic phenomena. Ann Phys. *Ann. Phys. (Paris).* 12:161–237.

30. Svergun, D. I. 1992. Determination of the regularization parameter in indirect-transform methods using perceptual criteria. *J. Appl. Crystallogr.* 25:495–503.

31. Eyal, E., R. Najmanovich, …, V. Sobolev. 2004. Importance of solvent accessibility and contact surfaces in modeling side-chain conformations in proteins. *J. Comput. Chem.* 25:712–724.

32. Svergun, D. I., C. Barberato, and M. H. J. Koch. 1995. CRYSOL: a program to evaluate x-ray solution scattering of biological macromolecules from atomic coordinates. *J. Appl. Crystallogr.* 28:768–773.

33. Varadi, M., S. Kosol, …, P. Tompa. 2014. pE-DB: a database of structural ensembles of intrinsically disordered and of unfolded proteins. *Nucleic Acids Res.* 42:D326–D335.

34. Uversky, V. N., J. R. Gillespie, and A. L. Fink. 2000. Why are "natively unfolded" proteins unstructured under physiologic conditions? *Proteins.* 41:415–427.

35. Ishida, T., and K. Kinoshita. 2008. Prediction of disordered regions in proteins based on the meta approach. *Bioinformatics.* 24:1344–1348.

36. Glotzer, M., A. W. Murray, and M. W. Kirschner. 1991. Cyclin is degraded by the ubiquitin pathway. *Nature.* 349:132–138.

37. Pfleger, C. M., and M. W. Kirschner. 2000. The KEN box: an APC recognition signal distinct from the D box targeted by Cdh1. *Genes Dev.* 14:655–665.

38. Dosztányi, Z., B. Mészáros, and I. Simon. 2009. ANCHOR: web server for predicting protein binding regions in disordered proteins. *Bioinformatics.* 25:2745–2746.

39. Uversky, V. N. 2012. Size-exclusion chromatography in structural analysis of intrinsically disordered proteins. *Methods Mol. Biol.* 896:179–194.

40. Schubert, M., D. Labudde, …, P. Schmieder. 2002. A software tool for the prediction of Xaa-Pro peptide bond conformations in proteins based on ^{13}C chemical shift statistics. *J. Biomol. NMR.* 24:149–154.

41. Jensen, M. R., G. Communie, …, M. Blackledge. 2011. Intrinsic disorder in measles virus nucleocapsids. *Proc. Natl. Acad. Sci. USA.* 108:9839–9844.

42. Cho, M. K., H. Y. Kim, …, M. Zweckstetter. 2007. Amino acid bulkiness defines the local conformations and dynamics of natively unfolded α-synuclein and τ. *J. Am. Chem. Soc.* 129:3032–3033.

43. Schwarzinger, S., G. J. Kroon, …, H. J. Dyson. 2001. Sequence-dependent correction of random coil NMR chemical shifts. *J. Am. Chem. Soc.* 123:2970–2978.

44. Wishart, D. S., C. G. Bigam, …, B. D. Sykes. 1995. ^{1}H, ^{13}C and ^{15}N random coil NMR chemical shifts of the common amino acids. I. Investigations of nearest-neighbor effects. *J. Biomol. NMR.* 5:67–81.

45. Kjaergaard, M., S. Brander, and F. M. Poulsen. 2011. Random coil chemical shift for intrinsically disordered proteins: effects of temperature and pH. *J. Biomol. NMR.* 49:139–149.

46. Tamiola, K., B. Acar, and F. A. Mulder. 2010. Sequence-specific random coil chemical shifts of intrinsically disordered proteins. *J. Am. Chem. Soc.* 132:18000–18003.

47. Mohana-Borges, R., N. K. Goto, …, P. E. Wright. 2004. Structural characterization of unfolded states of apomyoglobin using residual dipolar couplings. *J. Mol. Biol.* 340:1131–1142.

48. Ozenne, V., F. Bauer, …, M. Blackledge. 2012. Flexible-meccano: a tool for the generation of explicit ensemble descriptions of intrinsically disordered proteins and their associated experimental observables. *Bioinformatics.* 28:1463–1470.

49. Chao, W. C., K. Kulkarni, …, D. Barford. 2012. Structure of the mitotic checkpoint complex. *Nature.* 484:208–213.

50. Bernadó, P., and M. Blackledge. 2009. A self-consistent description of the conformational behavior of chemically denatured proteins from NMR and small angle scattering. *Biophys. J.* 97:2839–2845.

51. Click, T. H., D. Ganguly, and J. Chen. 2010. Intrinsically disordered proteins in a physics-based world. *Int. J. Mol. Sci.* 11:5292–5309.

52. Bernadó, P., and D. I. Svergun. 2012. Structural analysis of intrinsically disordered proteins by small-angle x-ray scattering. *Mol. Biosyst.* 8:151–167.

53. Viguera, A. R., and L. Serrano. 1999. Stable proline box motif at the N-terminal end of α-helices. *Protein Sci.* 8:1733–1742.

54. Tompa, P., and M. Fuxreiter. 2008. Fuzzy complexes: polymorphism and structural disorder in protein-protein interactions. *Trends Biochem. Sci.* 33:2–8.

55. Wright, P. E., and H. J. Dyson. 2009. Linking folding and binding. *Curr. Opin. Struct. Biol.* 19:31–38.

56. Knott, M., and R. B. Best. 2012. A preformed binding interface in the unbound ensemble of an intrinsically disordered protein: evidence from molecular simulations. *PLOS Comput. Biol.* 8:e1002605.

57. Ganguly, D., W. Zhang, and J. Chen. 2012. Synergistic folding of two intrinsically disordered proteins: searching for conformational selection. *Mol. Biosyst.* 8:198–209.

58. De Biasio, A., and F. J. Blanco. 2013. Proliferating cell nuclear antigen structure and interactions: too many partners for one dancer? *Adv Protein Chem Struct Biol.* 91:1–36.

59. Bowman, G. D., M. O'Donnell, and J. Kuriyan. 2004. Structural analysis of a eukaryotic sliding DNA clamp-clamp loader complex. *Nature.* 429:724–730.

60. Bruning, J. B., and Y. Shamoo. 2004. Structural and thermodynamic analysis of human PCNA with peptides derived from DNA polymerase-δ p66 subunit and flap endonuclease-1. *Structure.* 12:2209–2219.

61. Bubeck, D., M. A. Reijns, …, A. P. Jackson. 2011. PCNA directs type 2 RNase H activity on DNA replication and repair substrates. *Nucleic Acids Res.* 39:3652–3666.

62. Gulbis, J. M., Z. Kelman, …, J. Kuriyan. 1996. Structure of the C-terminal region of p21$^{\text{WAF1/CIP1}}$ complexed with human PCNA. *Cell.* 87:297–306.

63. Pascal, J. M., O. V. Tsodikov, …, T. Ellenberger. 2006. A flexible interface between DNA ligase and PCNA supports conformational switching and efficient ligation of DNA. *Mol. Cell.* 24:279–291.

64. Sakurai, S., K. Kitano, …, T. Hakoshima. 2005. Structural basis for recruitment of human flap endonuclease 1 to PCNA. *EMBO J.* 24:683–693.

65. Hammes, G. G., Y. C. Chang, and T. G. Oas. 2009. Conformational selection or induced fit: a flux description of reaction mechanism. *Proc. Natl. Acad. Sci. USA.* 106:13737–13741.

66. Hagai, T., A. Azia, …, Y. Levy. 2011. Intrinsic disorder in ubiquitination substrates. *J. Mol. Biol.* 412:319–324.

67. Kriwacki, R. W., L. Hengst, …, P. E. Wright. 1996. Structural studies of p21$^{\text{Waf1/Cip1/Sdi1}}$ in the free and Cdk2-bound state: conformational disorder mediates binding diversity. *Proc. Natl. Acad. Sci. USA.* 93:11504–11509.